

# Optical low-coherence reflectometry for deflection measurement with a fiber Bragg grating cantilever sensor

Ping Lu and Qiying Chen<sup>1</sup>

Department of Physics and Physical Oceanography, Memorial University of Newfoundland, St John's, NL A1B 3X7, Canada

E-mail: [qiyingc@mun.ca](mailto:qiyingc@mun.ca)

Received 1 January 2009, in final form 8 March 2009

Published 5 June 2009

Online at [stacks.iop.org/MST/20/075303](http://stacks.iop.org/MST/20/075303)

## Abstract

Optical low-coherence reflectometry (OLCR) for deflection measurement with a fiber Bragg grating (FBG) cantilever sensor is proposed and experimentally demonstrated to reveal the internal structure of the sensing fiber in correlation with its optical properties, which is the first report on a spatial-resolved technique to realize dynamic deflection measurement. The change in the fiber length during a convex or concave deflection of the cantilever sensor detected by OLCR achieves simultaneous determination of the magnitude and direction of the deflection by the use of a standard single-mode telecommunication fiber inscribed with single grating. The FBG plays a key role in selecting pre-strain set point and compensating the environmental temperature fluctuations. The experimental results are in good agreement with the theoretical analysis.

**Keywords:** optical fibers, fiber Bragg grating, sensor

(Some figures in this article are in colour only in the electronic version)

## 1. Introduction

Fiber-optic sensors have received considerable attention recently for their advantages such as immunity to electromagnetic interference, compact size, potential low cost and the possibility of distributed measurement over a long distance [1], which have been reported as powerful devices in sensing a wide range of environmental parameters including temperature, strain, pressure, displacement, humidity, salinity and saccharinity [1–8].

For practical applications, deflection sensors with merits of flexibility, light-weighted and versatility are highly demanded. Some published papers reported the use of deflections of optical fibers to realize measurement of different measurands, for example, high temperature [9], refractive index [10], force and displacement [11]. Fiber deflection sensors reported so far can be classified into three groups: (1) fiber-optic sensors on standard single-mode optical fibers

use the translucent protective sheath that encases a fiber as a means of locating small displacement on an otherwise straight fiber [12]. It is also possible to determine the deflection magnitude by measuring the reduction in the fiber's core light. (2) The second group consists of long-period gratings (LPGs), which are based on the detection of the fiber-orientation dependences of the spectral responses of special eccentric core fibers or D-shaped fibers [13, 14], multiple LPGs fabricated by different techniques [15], or fibers of cladding index modified by femtosecond lasers [16, 17]. (3) The third group comprises fiber Bragg gratings (FBGs) in which the sensing processes were achieved by the intrinsic sensitivity of the D-type fibers to curvature [18], by the tight transverse confinement of an axially offset FBG inscribed by an infrared femtosecond laser [19], or by combining a Mach–Zehnder interferometer with a cantilever-mounted FBG [20]. Among all reported sensors, direction-sensitive measurement has been achieved only on fibers with broken cylindrical symmetry in a few cases [13–16, 19] at the expense of high cost of the specialty fibers, expensive facilities to inscribe the fiber gratings, complicated processes

<sup>1</sup> Author to whom any correspondence should be addressed.



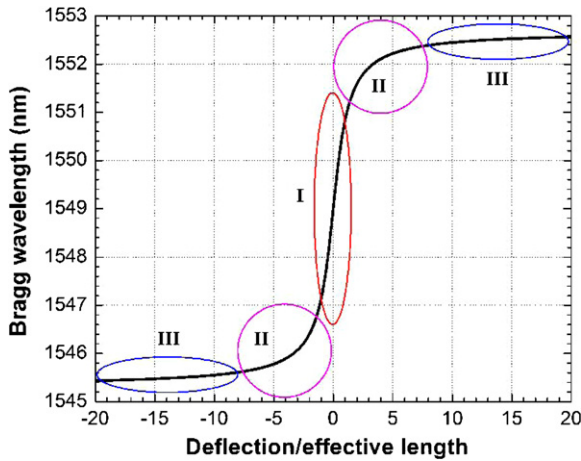


**Figure 3.** Simulation of the Bragg resonance wavelength as a function of the ratio of the deflection to the effective length.

deflection. The relationship between the change in the length of the fiber  $\Delta l$  and the deflection  $D$  is [21]

$$\Delta l = \frac{2dl}{L} \arctan\left(\frac{D}{L}\right), \quad (1)$$

where  $d$  is the neutral axis distance between the optical fiber and the cantilever, and  $L$  is the initial effective length of the cantilever. The shift of the Bragg resonance wavelength  $\Delta\lambda_B$  induced by the deflection is

$$\Delta\lambda_B = \frac{2d\lambda_B(1 - \hat{P}_e)}{L} \arctan\left(\frac{D}{L}\right), \quad (2)$$

where  $\hat{P}_e$  is an effective strain optic constant.

Figure 2(b) shows a schematic illustration of the fiber elongation due to a convex deflection of the cantilever. The operation principles of an FBG cantilever sensor have been discussed in our recent paper for application as a flow sensor [21]. Following (2), figure 3 simulates the Bragg wavelength ( $\lambda_B$ ) as a function of the ratio of the deflection to the effective length ( $D/L$ ). In addition to revealing the dependence of  $\lambda_B$  on the geometry of the cantilever, more information can be derived by judging the gradient of the curve at different  $D/L$  ratios, which is strongly related to the bending conditions of the cantilever sensor. Three segments can be identified on the curve, which are labeled as I, II and III. Segment I exhibits linear behavior for  $\Delta\lambda_B$  versus  $D/L$  when the FBG is stretched or compressed away from the pre-strained position within the proportionality limit. In segment III when the deflection goes beyond the limit, the Bragg wavelength approaches an extreme. Segment II is a transition region where the slope of the Bragg wavelength versus deflection/effective length decreases as it moves away from the proportionality region. When the FBG is attached to the cantilever, an optimal pre-strain value has to be chosen in order to satisfy the requirements of different deflection measurements. For a small deflection, a low pre-strained value is appropriate, however, an extremely low set point will result in nonlinear and nonsymmetrical performance of the sensor in the convex and concave deflection because the Bragg wavelength falls into segment II or even III due to a complete relaxation of the fiber. On the other hand, for

a large deflection, a high pre-strained value is suitable as long as it will not cause breakage of the FBG or relative movement between the coating and the cladding of the fiber. The set point of the pre-strained value for the FBG cantilever used in this study was  $100 \mu\epsilon$ , which was carefully selected to ensure that no break or relative movement between the fiber cladding and its polymeric coating takes place in the measurement.

### 3. Results and discussion

#### 3.1. In situ deflection monitoring with optical low-coherence reflectometry

OLCR is an interferometric technique to evaluate the structural and optical properties of materials and devices with a high spatial resolution, high reflection sensitivity and a large dynamical range [22–24]. A high-resolution reflectometer (Ando AQ7410B) with a sampling resolution of  $2 \mu\text{m}$  and a spatial resolution of  $20 \mu\text{m}$  was utilized to analyze the internal structure of the cantilever sensor in this study. As shown in the illustration of the OLCR measurement system (figure 1), a low-coherence LED light source (AQ7413, Yokogawa Electric Corp.) with peak wavelength at  $1.55 \mu\text{m}$  is launched into a fiber coupler and divided into two light paths in which part of light propagates into a test arm with the FBG while the other part is introduced to a reference arm where the optical delay is varied by the movement of a reference mirror. In the test arm, the light passes through a fiber adapter, the FBG, and to the cleaved fiber end immersed in an index-matching gel (IMG, Norland index matching liquid 150) where it is back reflected. The reflection from the FBG is recombined with the signal from the reference arm and received by the InGaAs photodetector. When the two optical path lengths are within the coherence length,  $L_C = \lambda^2/n\Delta\lambda$ , where  $n$  is the refractive index of the fiber core,  $\lambda$  and  $\Delta\lambda$  are the center wavelength and the spectrum bandwidth of the light source, respectively, the envelope of the interference signal can be detected. The location of the reflection can be obtained by precisely scanning the position of the moving mirror, while the reflectivity is measured by the intensity of the interference signal [25],

$$I(\tau) = R \left| \int_{-\infty}^{+\infty} S(\omega) I(\omega) e^{i\omega\tau} d\omega \right|, \quad (3)$$

where  $R$  is the responsivity of the photodetector,  $S(\omega)$  is the source spectral density,  $I(\omega)$  is the frequency-dependent reflectivity, and  $\tau$  is the time difference between the two arms.

Figure 4 plots the backscattered interferogram from the cantilever sensor as a function of fiber geometric length. A reflection peak of the Bragg grating appears between the peaks corresponding to the light reflected from the two ends of the fiber, i.e., the input air/fiber joint and the output fiber/IMG joint. A close-up of the three specific interferograms shown in figure 5 indicates that the corresponding peak reflectance/fiber geometric length are  $-14.65 \text{ dB}/4.344 \text{ mm}$ ,  $-32.83 \text{ dB}/848.25 \text{ mm}$  and  $-42.36 \text{ dB}/508.024 \text{ mm}$ , respectively. Several small peaks appear behind the strong grating (reflection 90%) region due to

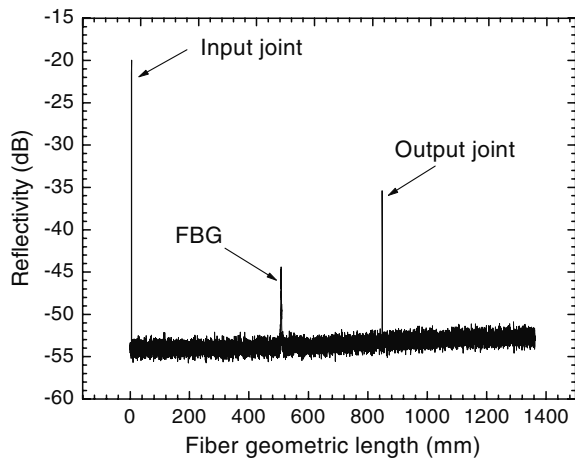


**Figure 4.** Low-coherence interferogram of the FBG used in this study. FBG is located between the air/fiber input facet and the fiber/IMG output facet.

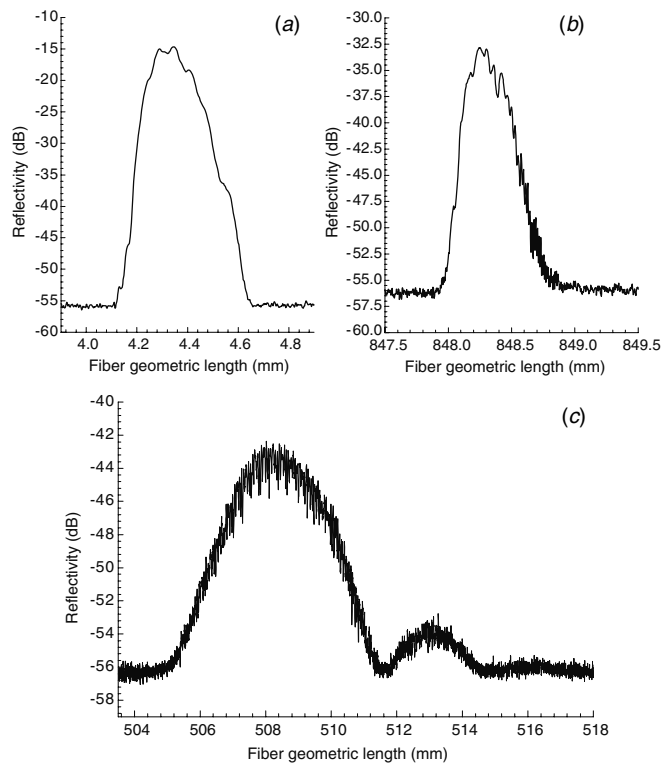


**Figure 5.** Interferogram close-up: (a) input air/fiber joint, (b) output fiber/IMG joint, and (c) FBG.

the strong multiple reflections [26]. Using the OLCR method to measure deflection with the cantilever sensor requires simultaneous monitoring of the reflected light from the two ends of the fiber. The reflection signals at these points are expected to be strong enough in order to obtain exact locations of the joints. In this study, the reflection at the input air/fiber joint through a fiber connector is  $-14.65$  dB, which is of suitable signal level to be distinguished from those at the FBG and the output joint. In other applications where the reflection at the input joint needs to be eliminated, fiber splicing may be adopted. Since the refractive index of the IMG is 1.52 (at

589 nm), which is slightly different from the corresponding value of 1.4682 (at 1550 nm) for the fiber core, the back-reflection carries a signal of  $-32.83$  dB, which is ideal for the application here to give a suitable signal level different from those reflections at the input air/fiber joint or at the grating section. In the case no IMG is used, the reflection from the output joint will be overwhelmingly greater than those from other locations, leading to difficulty in identification. In addition, the IMG can be used as an indication whether the fiber is intact or connected well during the experiment.

When the FBG sensor system was placed in a temperature-controlled room with the temperature maintained at  $20.0 \pm 1.0$  °C throughout the experiment, the top end of the cantilever was anchored onto a vertical frame and the bottom was contacted by a motor-driven linear stage (ATS100, Aerotech Inc.) with a motion accuracy of  $0.5$   $\mu\text{m}$  and a repeatability of  $0.3$   $\mu\text{m}$ . The experimental setup was similar to the one used in our recent paper on flow measurement [21] with the difference that the deflection effect was generated by the translation stage controlled by a computer through a general-purpose interface bus (GPIB) interface system and LabVIEW™ programming control instead of fluid flow. The translation stage moved forward from either side of the cantilever to change the deflection direction. When the translation stage moved from the side of the cantilever with the FBG, a convex deflection was induced on the cantilever and hence the FBG stayed in a stretched state. On the other hand, when the translation stage moved from the opposite side of the cantilever, the FBG experienced a concave deflection and stayed in a compressed state.

Since the two ends of the fiber with the grating section at the center were attached to the cantilever, the increase in the fiber output joint position corresponding to the elongation of the whole fiber was due to the deflection-induced extension of the fiber section between the two fixed points. For the FBG cantilever sensor, the thickness of the cantilever and the CPC coating diameter of the optical fiber were both  $250$   $\mu\text{m}$ . Thus the neutral axis distance between the cantilever and the optical fiber was  $250$   $\mu\text{m}$ . As illustrated in figure 1, the top section (30 mm) of the cantilever was fixed and the bottom section (10 mm) was pushed by the translation stage. The initial effective length of the cantilever  $L$  was 270 mm with an initial fiber attaching length  $l$  of 180 mm. When the translation stage, which was located at the same side of the fiber with respect to the cantilever, moved forward 100 mm with a step of 20 mm, the FBG experienced a convex deflection. An increase in the fiber length of 0.118 mm was observed. When the translation stage moved backward 20 mm with a step of 5 mm, the FBG experienced a concave deflection and a decrease in the fiber length of 0.025 mm was observed. In the case when the translation stage is moved backward further, the fiber departs from the cantilever surface and no further change in the fiber output joint position is observed due to the complete relaxation of the fiber. The fiber output joint position, which indicates the change in the fiber length as a function of the deflection, is shown in figure 6. The simulation obtained by using (1) exhibits good agreement with the experimental result. Figure 6 indicates that monitoring the change in the length of the

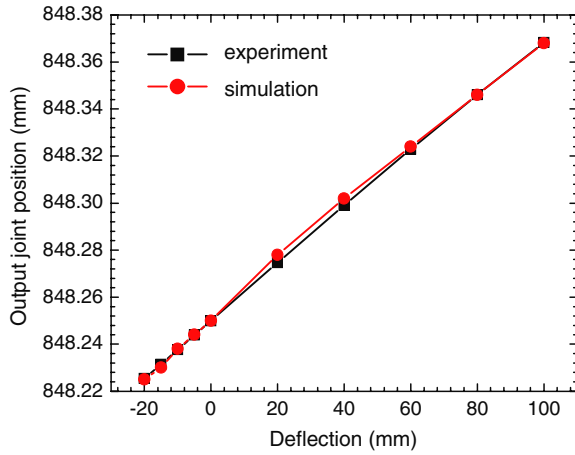


**Figure 6.** Dependence of the fiber output joint position on the deflection measured by optical low-coherence reflectometry. The shift in the fiber output joint position indicates the elongation of the fiber during deflection.

cantilever-supported fiber can distinguish both the magnitude and the direction of deflection by OLCR measurement.

### 3.2. Temperature compensation with fiber Bragg grating

If the variation of the environmental temperature in the space is not significant, the FBG can be placed away from the clamped section of the fiber on the cantilever. However, if the temperature variation is pronounced, it becomes necessary to place the FBG within the clamped section of the fiber in order to obtain more accurate temperature information by physically approaching the FBG to the testing area. The effects of the thermal expansions of the FBG and the cantilever as well as the cantilever length change induced fiber stretching on the FBG and the temperature and deflection coefficients of the fiber will be elucidated in the following paragraphs followed by a discussion on an approach to compensate the thermal effects.

The Bragg wavelength of the FBG as a function of temperature is shown in figure 7(a). The shift in the Bragg resonance wavelength of the grating due to a temperature fluctuation  $\Delta T$  can be expressed as  $\Delta\lambda_{B,T} = K_{T,\text{FBG}} \Delta T$ , where  $K_{T,\text{FBG}}$  is the temperature coefficient of the FBG, measured to be  $0.00975 \text{ nm } ^\circ\text{C}^{-1}$ . Figure 7(b) gives the experimental and simulated results on the dependence of the Bragg wavelength of the FBG cantilever sensor on deflection in both the convex and concave cases. At  $20^\circ\text{C}$ , a redshift in the FBG resonance peak wavelength over the convex deflection up to 90 mm was found to be  $0.716 \text{ nm}$ , which is close to the simulation value of  $0.727 \text{ nm}$  following (2). Operating in the region described by the linear segment I, the shift in the Bragg resonance wavelength of the grating due to a convex deflection  $D$  can be expressed as  $\Delta\lambda_{B,+D} = K_{+D,\text{FBG}} \Delta D$ , where  $K_{+D,\text{FBG}}$  is the convex deflection coefficient of the FBG, measured to be  $7.96 \times 10^{-3} \text{ nm mm}^{-1}$ . Similarly, a blueshift in the FBG resonance peak wavelength over the concave deflection up to 11 mm was  $0.097 \text{ nm}$ , which is close to the simulation value of  $0.100 \text{ nm}$ . The concave deflection coefficient of the FBG,  $K_{-D,\text{FBG}}$ , is measured to be  $8.82 \times 10^{-3} \text{ nm mm}^{-1}$ .

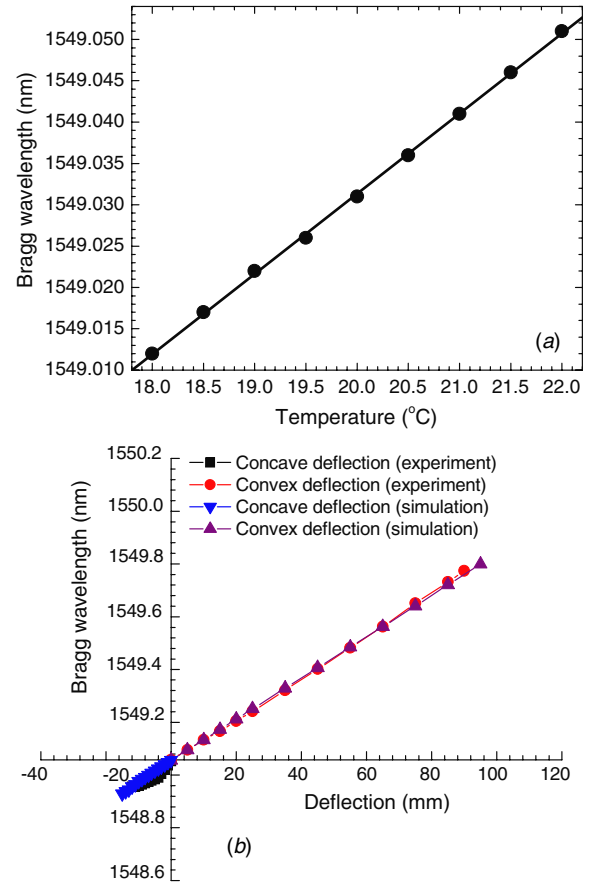


**Figure 7.** Dependence of the Bragg resonance wavelength of the cantilever-supported FBG on: (a) temperature around  $20^\circ\text{C}$ , and (b) convex and concave deflections, respectively.

The linear temperature expansion coefficient of the spring steel cantilever is about  $1.3 \times 10^{-5} \text{ mm } ^\circ\text{C}^{-1}$ , so the temperature coefficient of the 270 mm steel cantilever,  $K_{T,\text{stl}}$ , is  $3.51 \mu\text{m } ^\circ\text{C}^{-1}$  and the corresponding temperature coefficient of the 180 mm long fiber,  $K_{T,\text{stl-fib}}$ , is  $2.34 \mu\text{m } ^\circ\text{C}^{-1}$ . Since the fiber is CPC<sup>®</sup> coated fiber with a diameter of  $250 \mu\text{m}$  except the acrylate-recoated grating area of  $190 \mu\text{m}$  in diameter, the fiber grating area was not in contact with the steel cantilever directly when the two ends of the CPC coated fiber with the grating section at the center were mounted on the spring steel cantilever, as illustrated in figure 2. Consequently, the temperature variation around the cantilever and the fiber has no cross effect. The experimental result shows the convex and concave deflection coefficients of the fiber,  $K_{+D,\text{stl-fib}}$  and  $K_{-D,\text{stl-fib}}$ , are  $1.18 \times 10^{-3}$  and  $1.25 \times 10^{-3} \text{ mm mm}^{-1}$ , respectively. The temperature change around the cantilever has no significant effect on the deflection coefficients of the fiber and the FBG because of their small changes,  $\Delta K_{D,\text{stl-fib}}$  and  $\Delta K_{D,\text{FBG}}$ , which are about  $2 \times 10^{-6} \text{ mm mm}^{-1}$  and  $2 \times 10^{-5} \text{ nm mm}^{-1}$  for  $\Delta T$  of  $100^\circ\text{C}$  from (1) and (2), respectively.

Thus the change in the fiber length ( $\Delta l$ ) and the Bragg wavelength shift ( $\Delta\lambda_{\text{FBG}}$ ) can be expressed as

$$\begin{bmatrix} \Delta l \\ \Delta\lambda_{\text{FBG}} \end{bmatrix} = \begin{bmatrix} K_{T,\text{stl-fib}} & K_{D,\text{stl-fib}} \\ K_{T,\text{FBG}} & K_{D,\text{FBG}} \end{bmatrix} \begin{bmatrix} \Delta T \\ D \end{bmatrix}. \quad (4)$$

**Table 1.** Comparison of the OLCR method developed in this study with other recently reported bending/deflection measurement techniques

Parameter	LPG sensor in SMF [15]	D-shaped LPG sensor [14]	D-type FBG sensor [18]	Cantilever-mounted FBG sensor [20]	OLCR deflection sensor (this study)
Fiber	Corning SMF-28	D-shaped fiber	D-type fiber	SMF	Corning SMF-28
Sensing element	3 LPGs	2 LPGs	2 FBGs	1 FBG	1 FBG
Sensing mechanism	Shifts of LPG resonance wavelengths	Shifts of D-shaped LPG resonance wavelengths	Shifts of D-type FBG resonance wavelengths	Shifts in the FBG resonance wavelength	Rayleigh backscattering of reflected light
Sensitivity	Curvature sensitivity $5.2 \text{ nm m}^{-1}$	Curvature sensitivity $-2.5$ and $+2.85 \text{ nm m}^{-1}$	Curvature sensitivity depends on the radius of curvature	Deflection sensitivities $0.135 \text{ nm mm}^{-1}$ (vertical), and $0.602$ or $-0.572 \text{ nm mm}^{-1}$ (horizontal)	Direct deflection measurement, sampling resolution $2 \text{ }\mu\text{m}$
Accuracy	$-^b$	$0.4 \text{ m}^a$	$730 \text{ }\mu\text{m Hz}^{-1/2}$ at a measurement bandwidth of 1 Hz	$7.4 \text{ mm}$ (vertical); $1.7 \text{ mm}$ (horizontal) <sup>a</sup>	$20 \text{ }\mu\text{m}$
Temperature compensation	Impossible unless LPGs replaced by FBGs	$-^b$	Yes	Possible with one additional FBG	Yes
Detection limit	<ul style="list-style-type: none"> <li>Multiple LPGs prepared by different techniques</li> <li>Curvature and bending direction measured by different LPGs</li> </ul>	<ul style="list-style-type: none"> <li>Different bending sensitivities at different bend orientations</li> <li>Measurement at discrete fiber orientations</li> </ul>	<ul style="list-style-type: none"> <li>Non-Gaussian profile in FBG spectral response due to degradation</li> <li>Without vector-sensing capability</li> </ul>	<ul style="list-style-type: none"> <li>Complicated interrogation system</li> <li>Without vector-sensing capability</li> </ul>	Without vector-sensing capability

<sup>a</sup> Calculated from information available in the reference.

<sup>b</sup> Data not available.

Simultaneous measurement of the change in the fiber length and the Bragg wavelength shift of the FBG will provide a dynamic temperature compensation mechanism.

### 3.3. Effects of the mechanical properties of the cantilever

The adoption of an FBG in a cantilever configuration provides a capability to change the performance of the sensor system in addition to the obvious benefit of protection to the fiber. The neutral axis distance between the optical fiber and the cantilever is an important factor affecting the deflection sensitivity. The simulation of the dependence of the Bragg wavelength on the deflection under different neutral axis distances obtained by using (2) is shown in figure 8. The simulated shifts in the Bragg wavelength with the same 150 mm deflection for three neutral axis distances of  $250 \text{ }\mu\text{m}$ , 1 mm and 4 mm are 1.197, 4.787 and 23.935 nm, respectively. It is obvious that the Bragg wavelength of the FBG attached on the cantilever with a larger neutral axis distance will have a larger shift when the FBG sensor experiences the same deflection.

For the steel cantilever, the deflection at its end due to an external impaction force is [27]

$$D = \frac{F \cdot L^3}{3E \cdot I}, \quad (5)$$

where  $F$  is the force acting on the end of the cantilever,  $L$  is the length of the cantilever,  $E$  is Young's modulus of

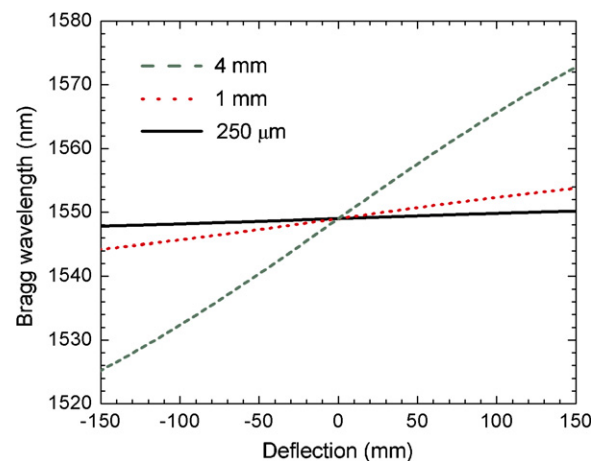


**Figure 8.** Simulation of the Bragg resonance wavelength as a function of deflection at different neutral axis distances of  $250 \text{ }\mu\text{m}$ , 1 mm and 4 mm, respectively.

the steel, and  $I$  is the area moment of the inertia for the cantilever. With the same force acting on the cantilever, the smaller the cantilever width, the larger the deflection will be. Therefore, the cantilever sensor with a large cantilever width is suited for measuring a small deflection and vice versa. The availability of different cantilever materials with various mechanical properties provides ample opportunity to design a sensor system satisfying specific requirements of applications.

### 3.4. Comparison between the OLCR method and other reported methods

For many applications of bend monitoring utilizing optical fibers, bending information must be indirectly recovered through proper determination of strain and subsequently transduction to bending. LPGs were found to possess better bend sensitivities than FBGs. However, LPGs are very sensitive to temperature, unable to operate on reflection, impossible for localized measurements, and difficult for embedding in composite materials [18]. In addition, their interrogation and multiplexing are not straightforward, which limit their practical applications. Even if the LPG sensor achieves simultaneous measurement of the magnitude and direction of a bend, a measurement independent of temperature and strain can only be achieved in the case that the LPGs are replaced by FBGs, when the cross-sensitivity between bend and temperature, or bend and strain, is resolved [15]. A comparison of the OLCR method developed in this study with other recently reported bending/deflection measurement techniques is listed in table 1, which indicates advantages of the OLCR method including direct deflection measurement, highest spatial accuracy, possible temperature compensation, possibility of quasi-distributed measurement, low cost and achievable with standard single-mode telecommunication fiber. The OLCR method realizes real-time spatial-resolved monitoring of deflection dynamics through direct deflection measurement, which is ideal for applications requesting highest spatial resolution or measurement in reflection mode. The OLCR method developed in this study does not possess vector-sensing capability to monitor fiber orientation, which could be achieved by the addition of fiber gratings or improvement in the interrogation system.

## 4. Conclusion

OLCR has been introduced to study the spatial-resolved dynamics of deflection with an FBG cantilever sensor and proved to be an effective technique in revealing the internal structure of the sensing fiber as well as realizing *in situ* deflection measurement for both magnitude and direction simultaneously. The interferograms of the OLCR measurement indicate the peak reflectance and fiber geometric length during the dynamic deflection measurement. An increase in the fiber length of 0.118 mm and a decrease of 0.025 mm were observed for the convex and concave deflection of the cantilever sensor with deflections of 100 and 20 mm, respectively. From the measurement of the FBG transmission spectrum, a temperature compensation mechanism is realized. The adoption of a FBG in a cantilever configuration provides an additional capability to change the performance of the sensor system in addition to the obvious benefit of protection to the fiber. The experimental results are in good agreement with the theoretical analysis. Some important aspects to design a suitable FBG cantilever sensor for different applications have been discussed, which include selection of pre-strain set point, effects of the mechanical properties of the cantilever and temperature compensation.

## Acknowledgments

The authors thank Natural Sciences and Engineering Research Council of Canada (NSERC) for the grant support to this research project. One of the authors (Q Chen) thanks Canada Research Chairs Program, Canada Foundation for Innovation, the Province of Newfoundland and Labrador, and the Memorial University of Newfoundland for the support of research infrastructure.

## References

- [1] Kuzyk M G 2006 *Polymer Fiber Optics: Materials, Physics, and Applications* (Boca Raton, FL: CRC)
- [2] Chin K K, Sun Y, Feng G, Georgiou G E, Guo K, Niver E, Roman H and Noe K 2007 Fabry–Perot diaphragm fiber-optic sensor *Appl. Opt.* **46** 7614–9
- [3] Dennison C R and Wild P M 2008 Enhanced sensitivity of an in-fibre Bragg grating pressure sensor achieved through fibre diameter reduction *Meas. Sci. Technol.* **19** 125301
- [4] Han M and Wang A 2006 Mode power distribution effect in white-light multimode fiber extrinsic Fabry–Perot interferometric sensor systems *Opt. Lett.* **31** 1202–4
- [5] Rogers J A, Kuo P, Ahuja A, Eggleton B J and Jackman E J 2000 Characteristics of heat flow in optical fiber devices that use integrated thin-film heaters *Appl. Opt.* **39** 5109–16
- [6] Lu P, Men L and Chen Q 2008 Resolving cross sensitivity of fiber Bragg gratings with different polymeric coatings *Appl. Phys. Lett.* **92** 171112
- [7] Men L, Lu P and Chen Q 2008 Intelligent multiparameter sensing with fiber Bragg gratings *Appl. Phys. Lett.* **93** 071110
- [8] Men L, Lu P and Chen Q 2008 A multiplexed fiber Bragg grating sensor for simultaneous salinity and temperature measurement *J. Appl. Phys.* **103** 053107
- [9] Nam S H and Yin S 2005 High-temperature sensing using whispering gallery mode resonance in bent optical fibers *IEEE Photon. Tech. Lett.* **17** 2391–3
- [10] Ng M N, Chen Z and Chiang K S 2002 Temperature compensation of long-period fiber grating for refractive-index sensing with bending effect *IEEE Photon. Tech. Lett.* **14** 361–2
- [11] Donlagić D and Culshaw B 2000 Propagation of the fundamental mode in curved graded index multimode fiber and its application in sensor system *IEEE J. Lightwave Technol.* **18** 334–42
- [12] Gauthier R C and Ross C 1997 Theoretical and experimental considerations for a single-mode fiber-optic bend-type sensor *Appl. Opt.* **36** 6264–73
- [13] Patrick H J 2000 Self-aligning, bipolar blend transducer based on long period grating written in eccentric core fiber *Electron. Lett.* **36** 1763–4
- [14] Zhao D, Chen X, Zhou K, Zhang L, Bennion I, MacPherson W N, Barton J S and Jones J D C 2004 Bend sensors with direction recognition based on long-period gratings written in D-shaped fiber *Appl. Opt.* **43** 5425–8
- [15] Wang Y P and Rao Y J 2005 A novel long period fiber grating sensor measuring curvature and determining bend-direction simultaneously *IEEE Sensors J.* **5** 839–43
- [16] Allsop T, Dubov M, Martinez A, Floreani F, Khrushchev I, Webb D J and Bennion I 2006 Bending characteristics of fiber long-period gratings with cladding index modified by femtosecond laser *IEEE J. Lightwave Technol.* **24** 3147–54
- [17] Allsop T, Dubov M, Martinez A, Floreani F, Khrushchev I, Webb D J and Bennion I 2005 Long period grating

- directional bend sensor based on asymmetric index modification of cladding *Electron. Lett.* **41** 59–60
- [18] Araujo F M, Ferreira L A, Santos J L and Farahi F 2001 Temperature and strain insensitive bending measurements with D-type fibre Bragg gratings *Meas. Sci. Technol.* **12** 829–33
- [19] Martinez A, Lai Y, Dubov M, Khrushchev I Y and Bennion I 2005 Vector bending sensors based on fibre Bragg gratings inscribed by infrared femtosecond laser *Electron. Lett.* **41** 472–4
- [20] Jin L, Zhang W, Li J, Zhang H, Liu B, Tu Q, Kai G and Dong X 2006 Two-dimensional bend sensing with a cantilever-mounted FBG *Meas. Sci. Technol.* **17** 168–72
- [21] Lu P and Chen Q 2008 Fiber Bragg grating sensor for simultaneous measurement of flow rate and direction *Meas. Sci. Technol.* **19** 125302
- [22] Giaccari Ph, Limberger H G and Salathé R P 2003 Local coupling-coefficient characterization in fiber Bragg gratings *Opt. Lett.* **28** 598–600
- [23] Hamel P, Jaouën Y, Gabet R and Ramachandran S 2007 Optical low-coherence reflectometry for complete chromatic dispersion characterization of few-mode fibers *Opt. Lett.* **32** 1029–31
- [24] Chapeleau X, Leduc D, Lupi C, Ny R Le, Douay M, Niay P and Boisrobert C 2003 Experimental synthesis of fiber Bragg gratings using optical low coherence reflectometry *Appl. Phys. Lett.* **82** 4227–9
- [25] Wiedmann U, Gallion P and Duan G 1998 A generalized approach to optical low-coherence reflectometry including spectral filtering effects *J. Lightwave Technol.* **16** 1343–7
- [26] Lambelet P, Fonjallaz P Y, Limberger H G, Salathé R P, Zimmer Ch and Gilgen H H 1993 Bragg grating characterization by optical low-coherence reflectometry *IEEE Photon. Tech. Lett.* **5** 565–7
- [27] Benham P P, Crawford R J and Armstrong C G 1996 *Mechanics of Engineering Materials* 2nd edn (Harlow, UK: Addison Wesley Longman) p 191